FUMIYOSHI TAKEDA*, TATSUYA YOSHINO*, YASUSHI UEMATSU**

DESIGN WIND FORCE COEFFICIENTS
FOR FREE-STANDING CANOPY ROOFS
OF MEMBRANE STRUCTURES

WSPÓŁCZYNNIKI PROJEKTOWE OBCIĄŻENIA
WIATREM DLA WOLNOSTOJĄCEGO DACHU
WYKONANEGO Z MEMBRANY

Abstract

The present study examines the wind-induced behaviour of free-standing membrane canopy roofs with various types of roof-supporting systems and presents wind force coefficients for designing such roofs. The effects of roof deformation and choice of roof-supporting system on wind force coefficients are investigated. The characteristics of wind-induced responses of the roofs are taken into account for improving the wind force coefficients that we previously proposed based on the results of wind tunnel experiment with rigid roof models.

Keywords: design wind force coefficients, membrane structure, structural analysis, computational fluid dynamics (CFD)

Streszczenie

W przedstawionych badaniach analizowane jest zachowanie wolnostojącego dachu membranowego, z różnymi systemami podparcia, poddanego oddziaływaniu wiatru. Zaprezentowano współczynniki użyteczne podczas projektowania takich dachów. Zbadano wpływ deformacji dachu oraz zastosowania różnych systemów wsporczych na współczynniki obciążenia wiatrem. W celu uzyskania poprawy współczynników sił pochodzących od wiatru, wcześniej zaproponowanych w oparciu o wyniki uzyskane eksperymentalnie w tunelu aerodynamicznym dla modelu ze sztywnym poszyciem dachu, uwzględniono charakterystyki odpowiedzi dachów na oddziaływanie wiatru.

Słowa kluczowe: współczynniki projektowe obciążenia wiatrem, konstrukcja membranowa, analiza konstrukcji, komputerowa mechanika płynów (CFD)

* Technical Research Center, Taiyo Kogyo Corporation, 3-20, Syodai-Tajika, Hirakatashi, Osaka, Japan.
** Department of Architecture and Building Science, Tohoku University, Sendai, Japan.

1. Introduction

Many free-standing canopy roofs of membrane structures are constructed to provide shade and weather protection in public spaces. Because they are lightweight and flexible, wind resistance is critical to their structural design. Regarding the wind loads on free-standing membrane canopy roofs, some studies have been carried out. For example, Pun and Letchford [5] analysed the response of an HP-shaped tension membrane roof subjected to fluctuating wind loads. Recently, Michalski et al. [1, 2] have shown an application of computational fluid dynamics (CFD) to the fluid-structure interaction (FSI) for a flexible umbrella structure. Nagai et al. [3] investigated the wind loads on a horn-shaped membrane structure. However, the number of studies on the design wind force coefficients of free-standing membrane canopy roofs is quite limited.

The authors proposed wind force coefficients for designing free-standing canopy roofs of various shapes based on wind tunnel experiments with rigid roof models [9, 10]. Assuming that four corner columns support the roof and that the roof deformation can be neglected, focus is on the axial forces induced in the columns. In practice, however, the roof deforms under wind loading, and roof-supporting systems other than four corner columns are also used. Takeda et al. [7, 8] showed that, in some cases, wind forces acting on the roof were significantly affected by the roof deformation and roof-supporting system. In this study, we propose design wind force coefficients for membrane roofs considering these two factors. Among the many roof configurations, we focus on mono-sloped and hyperbolic paraboloid (HP)-shaped roofs (Fig. 1).

Firstly, a brief explanation of the design wind force coefficients based on the wind tunnel experiments with rigid roofs is given. Then, the effects of roof deformation and type of roof-supporting system on the wind-induced responses are discussed. Finally, the design wind force coefficients for flexible membrane roofs are proposed.

Fig. 1. Free-standing canopy roofs of membrane structures, a) mono-sloped, b) HP-shaped

2. Definition of wind force and moment coefficients

2.1. Roof configurations

Figs. 2a and 3a show the tested roof configurations, where the mean roof height (H) of the mono-sloped roof and HP-shaped roofs are 6 m and 8 m, respectively.

2.2. Definition of wind force and moment coefficients

The definitions of the aerodynamic forces (D and L) and moments (M_x and M_y) are shown in Figs. 2b and 3b. The values of D, L, M_x and M_y for the mono-sloped and HP-shaped roofs are normalized using Eqns. (1) to (4) for mono-sloped roofs and Eqns. (5) to (8) for HP-shaped roofs, respectively,

$$C_D = \frac{D}{q_H \left(b^* l \sin\beta\right)} \qquad C_L = \frac{L}{q_H \left(bl\right)} \tag{1) (2}$$

$$C_{Mx} = \frac{M_x}{q_H \left(bl^2\right)} \qquad C_{My} = \frac{M_y}{q_H \left(b^{*2} l\right)} \tag{3) (4}$$

$$C_D = \frac{D}{q_H ha} \qquad C_L = \frac{L}{q_H S} \tag{5) (6}$$

$$C_{Mx} = \frac{M_x}{q_H Sa} \qquad C_{My} = \frac{M_y}{q_H Sa} \tag{7) (8}$$

where q_H is the reference velocity pressure at mean roof height H. For the mono-sloped roofs, b represents the horizontal (projection) width of the roof, while b^* ($= l$) represents the actual width of the roof (Fig. 2). For the HP-shaped roofs, h represents the difference in height of the roof, a represents the horizontal (projection) width of the roof, and S represents the projection area of the roof.

For simplicity, the design wind force coefficients on the roof are specified by two uniformly distributed values (C_{NW} and C_{NL}) over the windward and leeward halves, which are defined in terms of the velocity pressure q_H at the mean roof height.

The wind force coefficients are

$$C_{NW} = \frac{N_W}{q_H \left(b^* l / 2\right)} \qquad C_{NL} = \frac{N_L}{q_H \left(b^* l / 2\right)} \tag{9) (10}$$

for the mono-sloped roof and

$$C_{NW} = \frac{N_W}{q_H(S/2)} \quad C_{NL} = \frac{N_L}{q_H(S/2)} \tag{11}(12)$$

where N_W and N_L respectively represent the normal positive downward wind forces, on the windward and leeward halves. The coefficients C_{NW} and C_{NL} are given by Eqns. (13) and (14) for mono-sloped roof and by Eqns. (15) and (16) for HP-shaped roofs.

$$C_{NW} = -C_L - 4C_{My} \quad C_{NL} = -C_L + 4C_{My} \tag{13}(14)$$

$$C_{NW} = -C_L - 3\sqrt{2}C_{My} \quad C_{NL} = -C_L + 3\sqrt{2}C_{My} \tag{15}(16)$$
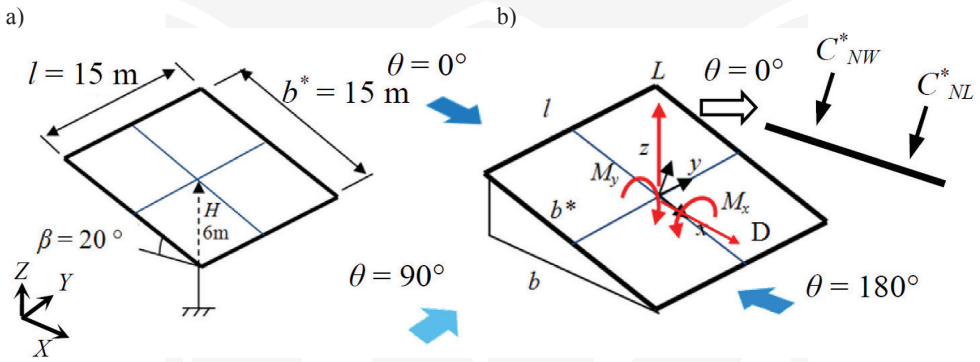
a) b)

Fig. 2. Mono-sloped free roof, a) configuration, b) definitions
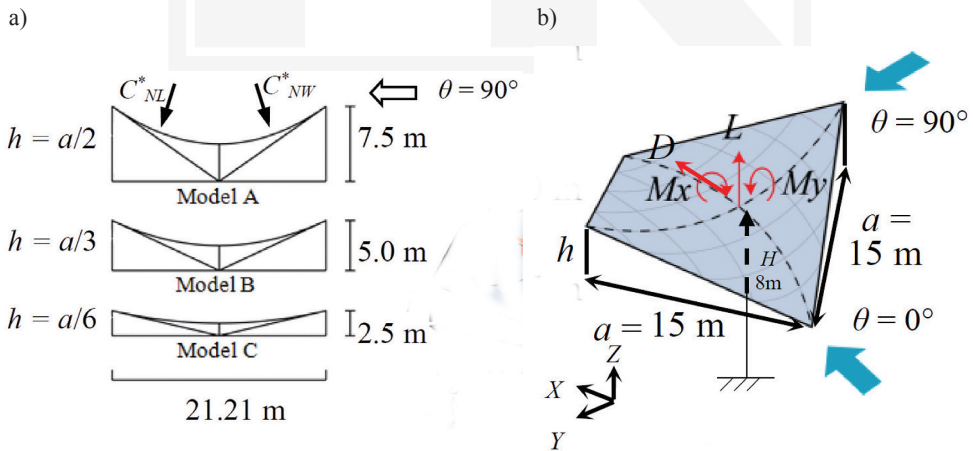
a) b)

Fig. 3. Hyperbolic paraboloid-shaped free roofs, a) configuration, b) definitions

3. Design wind force coefficients for rigid free roofs

In a previous study [10], the design wind force coefficients C^*_{NW} and C^*_{NL} for mono-sloped and HP-shaped rigid roofs were specified by Eqns. (17) and (18),

$$C^*_{NW} = \frac{\gamma C_{NW0}}{G_f} \qquad C^*_{NL} = \frac{\gamma C_{NL0}}{G_f} \qquad\qquad (17)\,(18)$$

where C_{NW0} and C_{NL0} represent the basic values of C_{NW} and C_{NL} for $\theta = 0°$ and $180°$ in the mono-sloped roof case and for $\theta = 0°$ and $90°$ in the HP-shaped roof case. They are computed by using a combination of C_L and C_{My} (or C_{Mx}) at an apex of the hexagon as shown in Fig. 4, which approximates the envelope of the C_L–C_{My} (or C_L–C_{Mx}) trajectory obtained from the wind tunnel experiments (see Fig. 5). A gust effect factor (G_f) of 2.0 based on the load effect is used. A correction factor (γ) is used for considering the effect of wind direction. Two sets of C_{NW0} and C_{NL0} values are selected from the six sets corresponding to the apexes, which produce the maximum tension and compression in the columns.
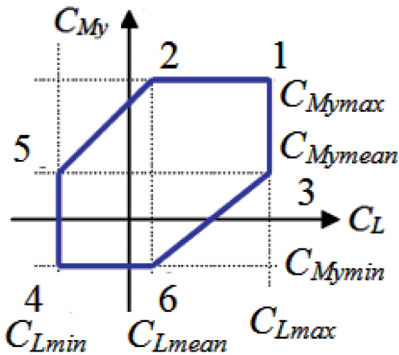

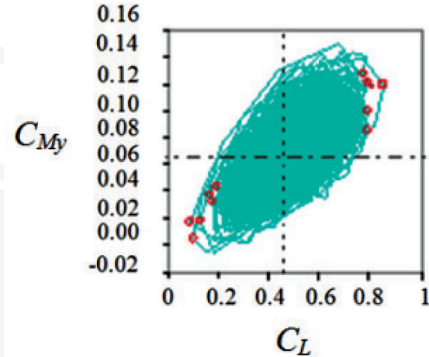
Fig. 4. Model of the envelope of the C_L and C_{My} Fig. 5. Time history of the C_L–C_{My} trajectory

4. Roof-supporting systems of membrane structures

4.1. Analytical models

Structural analysis was performed by using a finite-element method (FEM) to investigate how the roof-supporting system of membrane roofs affected the load effects. Figs. 6a–6c and 7a–7c show analytical models for mono-sloped roof of $\beta = 20°$ and HP-shaped roof of $h = a/2$ with different roof-supporting systems, respectively. Frame and suspension types are often used in membrane structures. The F1 and F2 models in Figs. 6 and 7 represent

frame types, whereas the S1 model represents a suspension type. In the F1 model, the roof structure consists of perimeter girders and binding beams. The roof frame is covered with a pre-tensioned membrane. The F2 model consists of perimeter girders and pre-tensioned membrane (Figs. 6b and 7b). In the F1 and F2 models, four corner columns support the roof girders. The S1 model consists of curved perimeter cables and pre-tensioned membrane. The roof is supported by posts and guy cables at the four corners. The column bases of the F1 and F2 models are fixed, whereas the posts of the S1 models are pin-supported. The roof area of the S1 model is approximately 82% of that of the frame models because of the curved perimeter. The S1 model is the most flexible of the three, which causes the roof to deform the most under wind loading. On the other hand, the F1 model is relatively rigid. Moreover, the roof membrane slightly deforms in the downward direction owing to its weight. Therefore, the initial shapes of these three roofs slightly differ from each other because of the difference in the supporting system. The pre-stress is 4 kN/m in the warp and fill (weft) directions of the membrane. The self-weight of the membrane is 12 N/m².
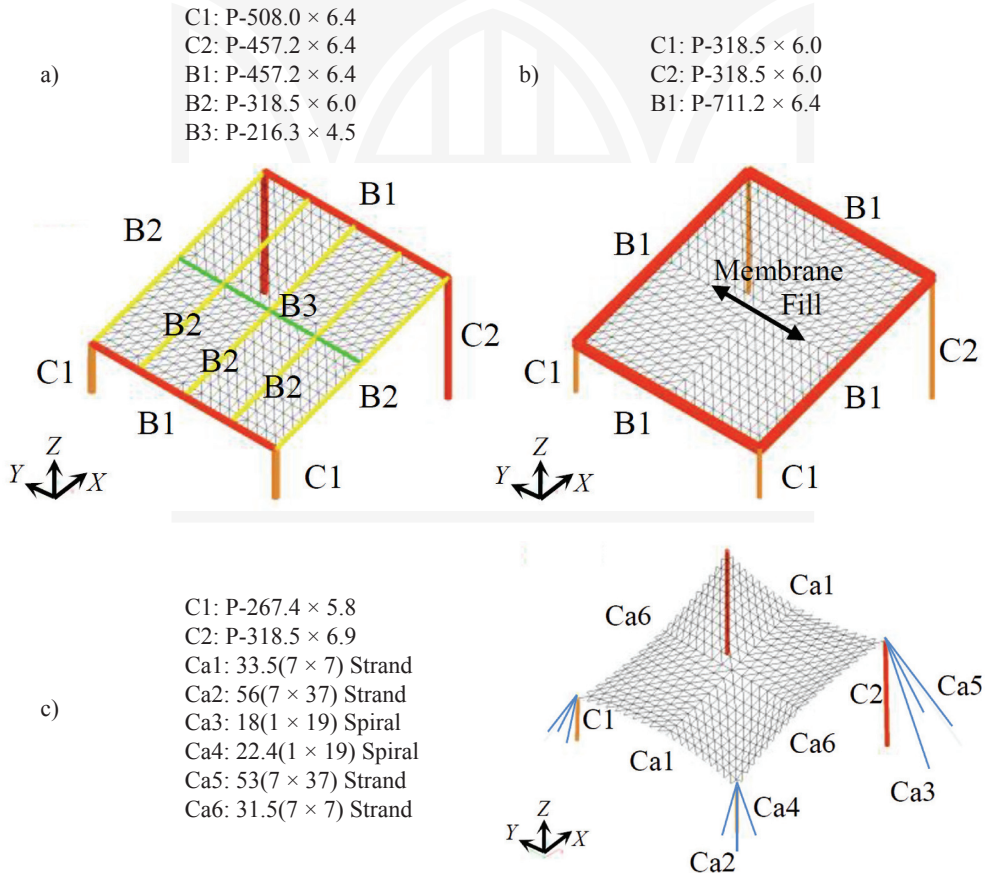
Fig. 6. Mono-sloped roof structural models, a) frame type 1 (F1), b) frame type 2 (F2), c) suspension type (S1)
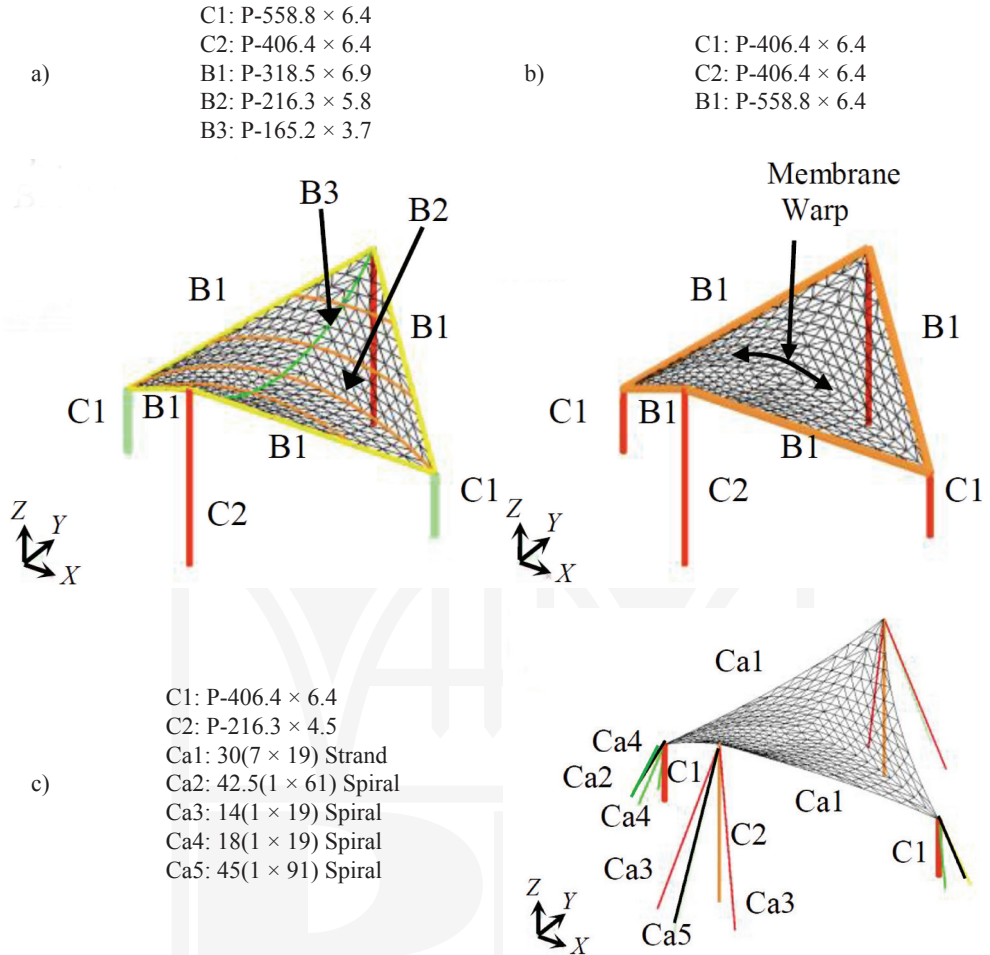
a)

C1: P-558.8 × 6.4
C2: P-406.4 × 6.4
B1: P-318.5 × 6.9
B2: P-216.3 × 5.8
B3: P-165.2 × 3.7

b)

C1: P-406.4 × 6.4
C2: P-406.4 × 6.4
B1: P-558.8 × 6.4

c)

C1: P-406.4 × 6.4
C2: P-216.3 × 4.5
Ca1: 30(7 × 19) Strand
Ca2: 42.5(1 × 61) Spiral
Ca3: 14(1 × 19) Spiral
Ca4: 18(1 × 19) Spiral
Ca5: 45(1 × 91) Spiral

Fig. 7. HP-shaped roof structural models, a) frame type 1 (F1), b) frame type 2 (F2), c) suspension type (S1)

4.2. Structural analysis

Structural analysis was carried out by using the in-house Taiyo Kogyo Corporation MAGESTIC software. The program is based on FEM, in which the geometrical non-linearity and the Newton–Raphson method are taken into account. The membrane material is assumed to be orthotropic and elastic. Furthermore, we assume that the membrane only carries tension; in other words, it does not resist compression and bending moment. The design wind speed is 31.5 m/s and the corresponding velocity pressure is 605 N/m². Wind force coefficients based on wind tunnel experiments with rigid models were used for computing the wind loads, which are the six sets of C_L and C_{My} corresponding to the apexes of the hexagon shown in Fig. 4.

Tables 1 and 2 summarize the wind force coefficients for the mono-sloped and HP-shaped roofs, respectively. We have adopted the correction factor $\gamma = 1.0$ because the maximum tension and compression are induced when $\theta = 0°$ and $\theta = 180°$ for the mono-sloped roof and when $\theta = 0°$ and $\theta = 90°$ for the HP-shaped roof. We take the gust effect factor $G_f = 2.0$ for evaluating the design wind force coefficients.

Table 1

Wind force coefficients for the mono-sloped roofs

Apex	Combination of C_L and C_{My}	Wind direction $\theta = 0°$		Wind direction $\theta = 180°$	
		C_{NW0}	C_{NL0}	C_{NW0}	C_{NL0}
1	$C_{Lmax} + C_{Mymax}$	−2.45	−0.19	0.19	0.50
2	$C_{Lmean} + C_{Mymax}$	−1.96	0.30	0.65	0.96
3	$C_{Lmax} + C_{Mymean}$	−1.93	−0.71	−0.13	0.83
4	$C_{Lmin} + C_{Mymin}$	−0.51	−0.20	0.59	2.76
5	$C_{Lmin} + C_{Mymean}$	−0.96	0.25	1.20	2.16
6	$C_{Lmean} + C_{Mymin}$	−0.99	−0.68	−0.28	1.89

Table 2

Wind force coefficients for the HP-shaped roofs

Apex	Combination of C_L and C_{My}	Wind direction $\theta = 0°$		Wind direction $\theta = 90°$	
		C_{NW0}	C_{NL0}	C_{NW0}	C_{NL0}
1	$C_{Lmax} + C_{Mymax}$	−0.65	−0.72	−0.37	0.11
2	$C_{Lmean} + C_{Mymax}$	−0.31	−0.38	0.02	0.50
3	$C_{Lmax} + C_{Mymean}$	−0.40	−0.97	−0.89	0.63
4	$C_{Lmin} + C_{Mymin}$	0.80	−0.67	−0.56	2.31
5	$C_{Lmin} + C_{Mymean}$	0.35	−0.22	0.12	1.63
6	$C_{Lmean} + C_{Mymin}$	0.39	−1.08	−1.17	1.70

Table 3

Membrane (t: thickness)

Tensional stiffness	$E_w \times t = 1284.67$ kN/m (Warp) $E_f \times t = 861.024$ kN/m (Fill)
Poisson's ratio	$v_w = 0.85$ (Warp) $v_f = 0.57$ (Fill)
Shear modulus	$G \times t = 57$ kN/m

Note: Measured by 'MSAJ/M-02 1995' and 'MSAJ/M-01 1993' in the Standards of the Membrane Structures Association of Japan.

T a b l e 4

Cable

Elastic modulus	$E = 1.37 \times 10^8$ kN/m^2 (Strand)
	$E = 1.57 \times 10^8$ kN/m^2 (Spiral)

T a b l e 5

Beam and Post

Elastic modulus	$E = 2.05 \times 10^8$ kN/m^2
Poisson's ratio	$\nu = 0.3$

In the structural analysis, the stresses involved in the members are calculated based on the Building Standard Law of Japan and the design standard for steel structures. For the membranes and cables, tensile stresses are calculated from the tensile forces; for the beams and columns, the extreme fibre stresses are calculated by combining the axial force and bending moment; the axial stresses involved in the posts of the S1 model are calculated from the axial forces. The allowable stresses and material constants are also determined based on the Building Standard Law. Tables 3–5 summarize the material constants. Moreover, the ratio of the computed stress to the allowable stress is calculated and we call it the 'stress ratio'. Each member size is determined so that the stress ratios become less than 1.0.

4.3. Load effect

The design wind force coefficients C^*_{NW} and C^*_{NL} were proposed assuming that the roof was rigid and supported by four corner columns, focussing on the column axial forces as the load effect. The wind force coefficients provide the maximum tension and compression on the columns, which correspond to the wind loads at the two apexes of the hexagon shown in Fig. 4. For the rigid mono-sloped roofs, apexes 1 and 4 provide the maximum load effects, whereas apexes 3 and 6 are applicable to the rigid HP-shaped roofs. However, in the case of membrane structures, the roof is so flexible that it cannot be considered rigid. Furthermore, the roof-supporting system may differ from that assumed in the previous study. Wind forces acting on the roof are first transferred to the peripheral members (beams or cables) via the membrane tension and thereafter, they are transferred to the columns or the post and guy cables. Therefore, load effects other than the column axial forces should also be considered for such structures. This subject is discussed below based on the structural analysis.

Figs. 8–10 and 11–13 show the results of the structural analysis for the F1, F2 and S1 models of the mono-sloped and HP-shaped roofs, respectively. In these figures, the maximum stress ratios for the members, i.e. membrane (Mem), cable, column, beam and post, are shown for the six apexes of the hexagon in Fig. 4. The maximum stress ratios are given at one of the two apexes providing the design wind force coefficients obtained from wind tunnel experiments with rigid models. However, these combinations are not sufficient for providing the maximum stress ratio. Tables 6 and 7 summarize such cases.
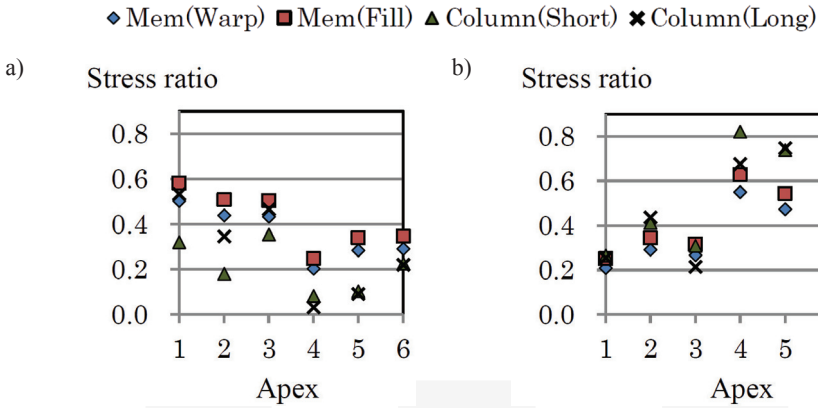
◆ Mem(Warp) ■ Mem(Fill) ▲ Column(Short) ✖ Column(Long)

a) Stress ratio   b) Stress ratio

Fig. 8. Stress ratio for the F1 model of the mono-sloped roof, wind direction a) θ = 0°, b) θ = 180°

◆ Mem(Warp) ■ Mem(Fill) ▲ Column(Short) ✖ Column(Long)

a) Stress ratio   b) Stress ratio
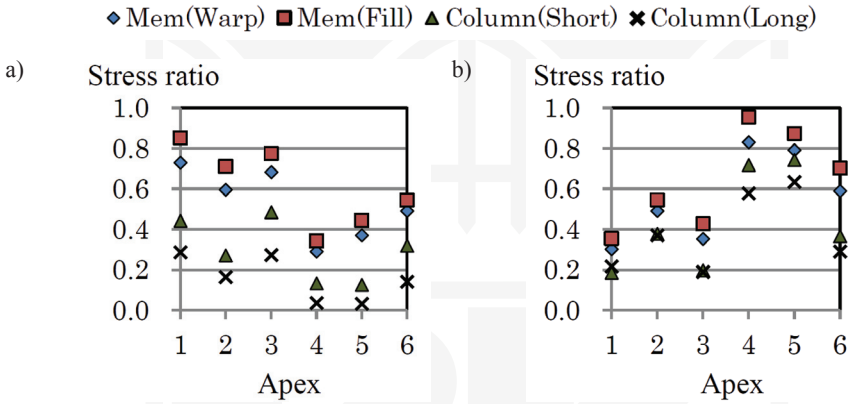
Fig. 9. Stress ratio for the F2 model of the mono-sloped roof, wind direction a) θ = 0°, b) θ = 180°

◆ Mem(Warp) ■ Mem(Fill) ▲ Column(Short) ✖ Column(Long)

a) Stress ratio   b) Stress ratio
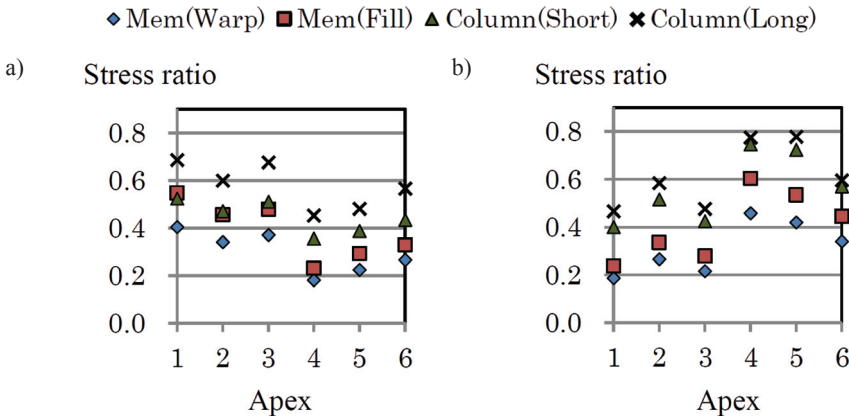
Fig. 10. Stress ratio for the S1 model of the mono-sloped roof, wind direction a) θ = 0°, b) θ = 180°
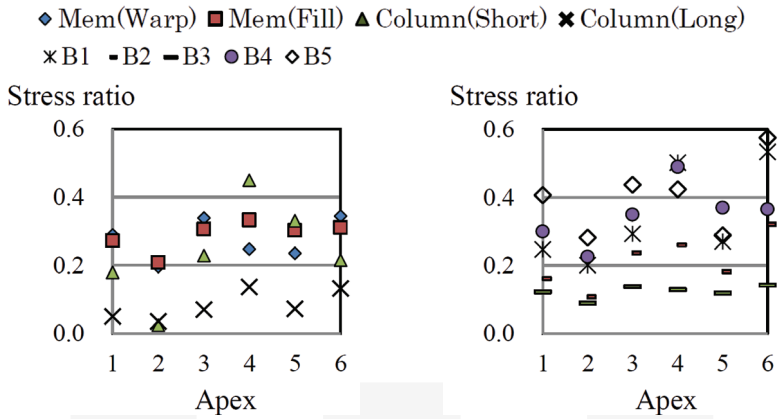
◆ Mem(Warp) ■ Mem(Fill) ▲ Column(Short) ✖ Column(Long)

✳ B1 ┅ B2 ━ B3 ● B4 ◇ B5

Fig. 11. Stress ratio for the F1 model of the HP-shaped roof, wind direction θ = 0°

◆ Mem(Warp) ■ Mem(Fill) ▲ Column(Short) ✖ Column(Long)

✳ B1

Fig. 12. Stress ratio for the F1 model of the HP-shaped roof, wind direction θ = 0°

◆ Mem(Warp) ■ Mem(Fill) ▲ Column(Short) ✖ Column(Long)
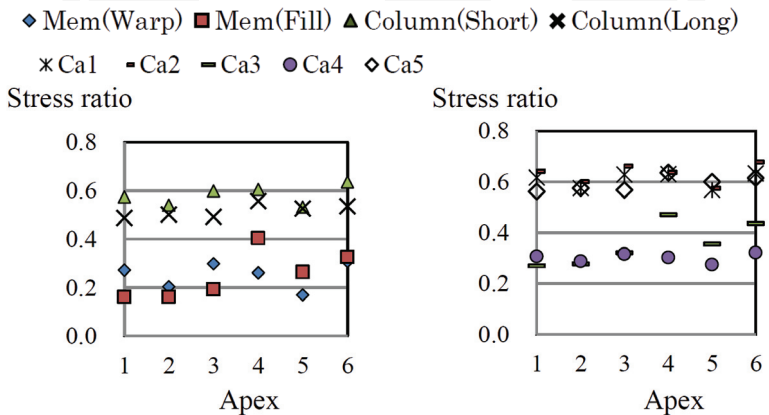
✳ Ca1 ┅ Ca2 ━ Ca3 ● Ca4 ◇ Ca5
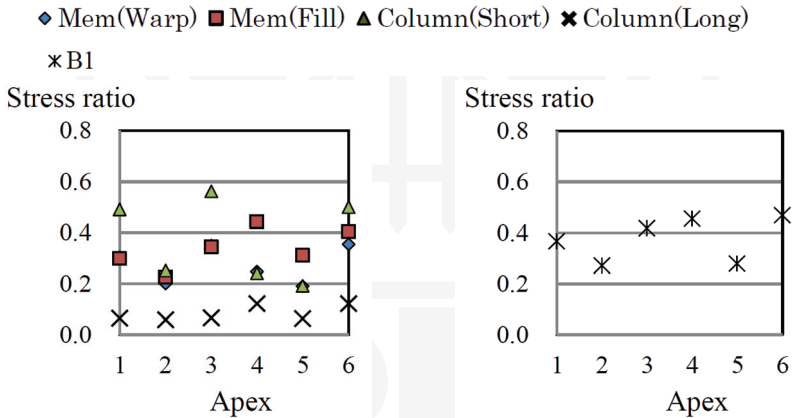
Fig. 13. Stress ratio for the S1 model of the HP-shaped roof, wind direction θ = 0°

Stress ratios for the mono-sloped roof

a) Wind direction θ = 0°

Member		Stress ratio			Ratio of
		Apex 1	Apex 4	Apex 3	Apex 3 to 1 or 4
F1	C1	0.32	0.08	0.35	1.11
F2	C1	0.44	0.13	0.49	1.10
S1	Ca3	0.58	0.46	0.61	1.06
	Ca4	0.50	0.36	0.54	1.07

b) Wind direction θ = 180°

Member		Stress ratio			Ratio of
		Apex 1	Apex 4	Apex 5	Apex 5 to 1 or 4
F1	C2	0.25	0.68	0.75	1.11
F2	C1	0.19	0.72	0.74	1.03
	C2	0.22	0.58	0.64	1.10
S1	C2	0.47	0.77	0.78	1.01

Stress ratios for the HP-shaped roof

Wind direction θ = 0°

Member		Stress ratio			Ratio of
		Apex 3	Apex 4	Apex 6	Apex 6 to 3 or 4
F1	Mem (Warp)	0.34	0.25	0.34	1.02
	B2	0.29	0.50	0.53	1.06
	B3	0.44	0.42	0.58	1.32
F2	Mem (Warp)	0.35	0.25	0.35	1.01
	B1	0.42	0.46	0.47	1.03
S1	Mem (Warp)	0.30	0.26	0.31	1.03
	Ca1	0.63	0.63	0.63	1.01
	Ca2	0.66	0.64	0.68	1.06
	Ca4	0.32	0.30	0.32	1.03
	C1	0.60	0.60	0.64	1.02

4.4. Combination of lift and aerodynamic moment coefficients providing the maximum values for various load effects

It was shown in the previous section that the two apexes corresponding to the design wind force coefficients for rigid roofs do not always give the maximum stress ratio. This cause may

be related to (i) the bending moment, (ii) the roof-supporting system and (iii) the direction of wind resultant force vector induced by the roof deformation.

Firstly, we consider the effect of the bending moment. Fig. 14 shows the maximum stress ratios for the axial force, bending moment and their combination that are induced in the C1 columns of the F2 model with mono-sloped roof. The figure shows that the stress ratio for the bending moment dominates the maximum stress ratios. This is also observed in the HP-shaped roofs. Therefore, the bending moment may affect the proposed design wind force coefficients because the maximum stress ratio is provided by the combination of the extreme fibre stress of bending moment and the axial stress. This feature implies that not only the column axial forces but also other load effects, such as the bending moment, should be considered when discussing the design wind force coefficients for membrane roof structures.

Secondly, we consider the roof-supporting system. There are various roof-supporting systems for membrane roofs. Figs. 15a–15c show examples of roof-supporting systems for mono-sloped roofs. In these figures, the arrows show the flow of the wind load (i.e. load pass) from the roof to the ground. The type-1 model is obtained by removing the B3 member from the F1 model (Fig. 6a); therefore, the structure and load pass of type-1 are similar to those of F1. Wind loads acting on the roof of type-1 are transferred from the roof to the ground via the gate-shaped frames with the horizontal beam. On the other hand, in type-3 model, the roof girders are disposed in a direction perpendicular to those of the type-1; therefore, the load pass is different as shown in Fig. 15c. The type-2 model is a combination of type-1 and type-3; the wind loads flow to the perimeter girders. Fig. 16a shows the roof girders for the type-1 model, in which the wind load distributed along the girder for $\theta = 0°$ is also shown. Vertical reactions are induced at the edges of the girders by the wind loads. These reactions act on the gate-shaped frames in the opposite direction, as shown in Fig. 16b. Figs. 17a and 17b show the wind force coefficients corresponding to the apex 1 (AP1) and apex 3 (AP3), respectively. The wind load corresponding to AP1 provides the design wind force coefficients proposed by Uematsu et al. (2008). However, the maximum load effects are attributed to the wind load corresponding to AP3 (see Table 6a) because of the difference in the vertical reaction at the edge B of the girder between AP1 and AP3. The value of reaction at the edge point B for AP3 is about 1.35 times greater than that for AP1. As a result, the bending moment for AP3 is greater than that for AP1 (Fig. 16c). Therefore, the wind load corresponding to AP3 produces the maximum load effects.
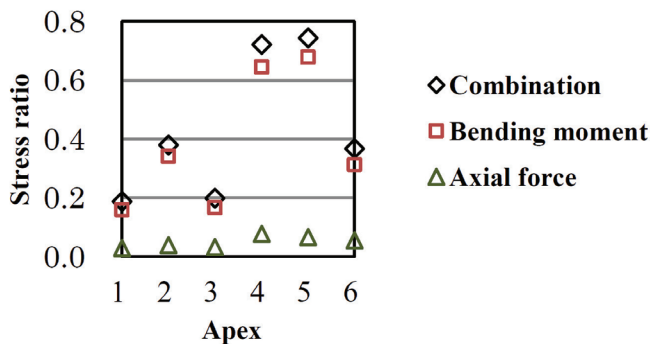

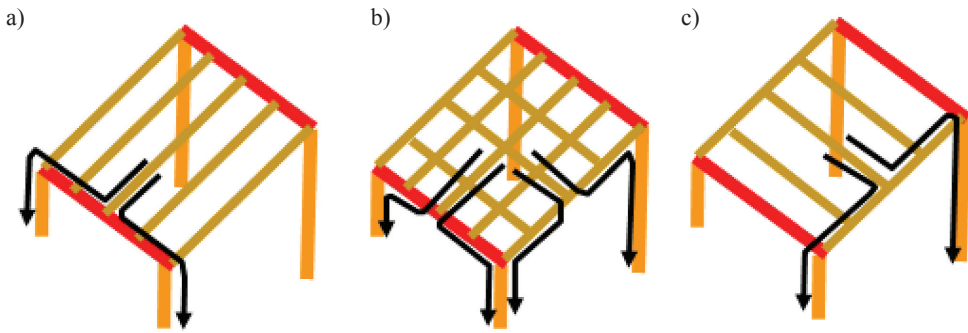Fig. 14. Stress ratios for the bending moment, axial force and combinations

a) b) c)

Fig. 15. Various roof-supporting systems for the mono-sloped roof and load flows, a) type-1, b) type-2, c) type-3
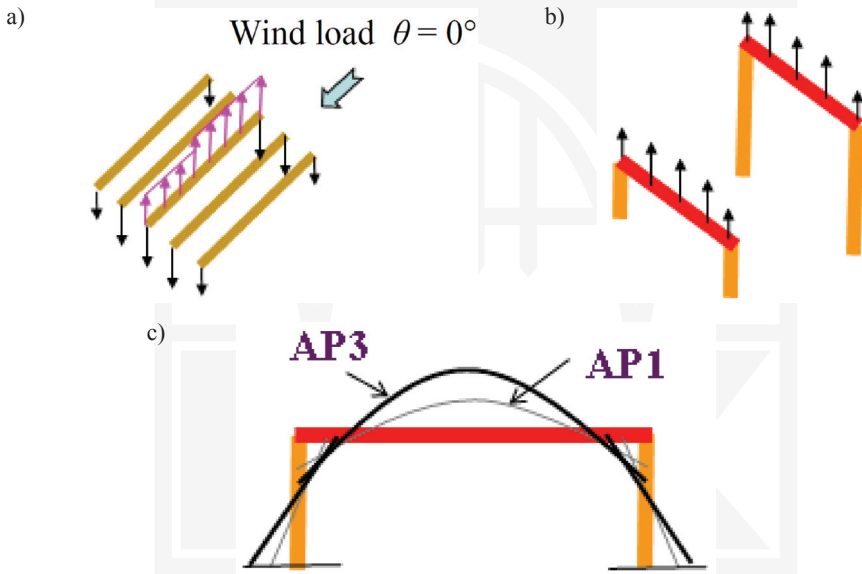
a) Wind load $\theta = 0°$ b)

c) AP3 AP1

Fig. 16. Load flows and resultant bending moments, a) wind load applied to roof girders, b) wind load applied to gate-shaped frame, c) bending moments

Thirdly, we consider the roof deformation. The membrane roofs are composed of triangular elements in the FEM analysis. The wind pressure is uniform in each triangular element. The wind force vector is obtained by integrating the distributed wind load, as shown in Fig. 18a. This vector is perpendicular to the surface of the triangle. The resultant force vector for the wind load is obtained by adding the wind force vectors of the triangular element of the roof. Figs. 18b and 18c show the deformed roof shapes of the F2 model for the mono-sloped roof that correspond to the wind loads corresponding to AP1 and AP3, respectively. The resultant force vectors are also shown in the figures. The absolute values of the X, Y and Z components for the resultant force vector can be found from the total value of each reaction force at the

supporting point of the columns, because it is necessary to balance the total reaction forces and the total external force (i.e. the wind force). Table 8 shows the X and Z components of the total reaction forces of the F1 and F2 models at AP1 and AP3 when wind direction is $\theta = 0°$. Comparing the reaction forces X (i.e. horizontal force) for AP1 and AP3 with each other, we can find that the value for AP3 is greater than that for AP1; i.e. the resultant force vector of the wind load for AP3 is more inclined to the ground compared with that for AP1, as shown in Fig. 18c. The greater horizontal force for AP3 induces additional bending moment by multiplying the horizontal force by the distance between the acting point of the vector and the ground. As a result, the wind load corresponding to AP3 is responsible for the maximum load effects. From the above discussion, we should improve the proposed design wind force coefficients for rigid roofs.
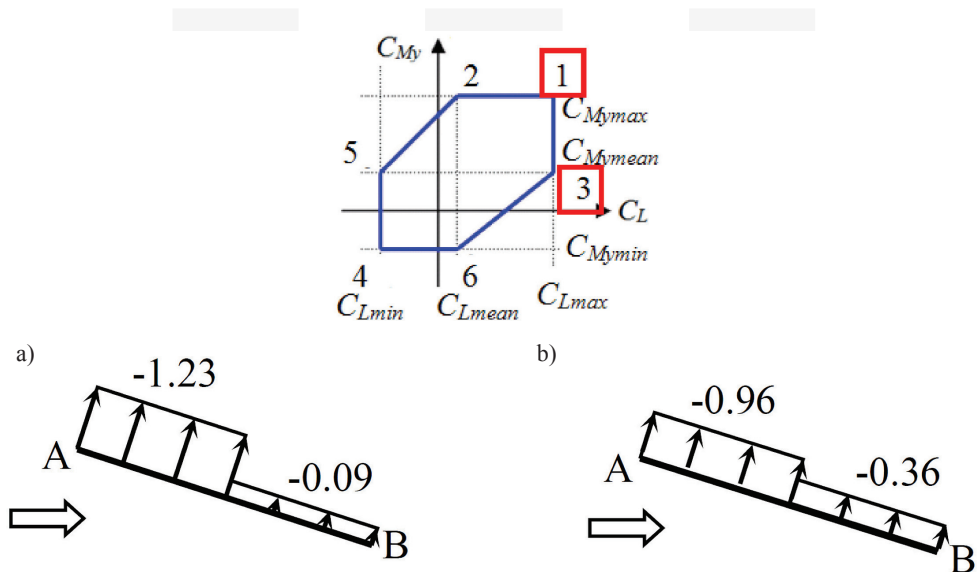

a)

b)

Fig. 17. Differences in the distribution of wind force coefficients between AP1 and AP3, wind direction $\theta = 0°$, a) AP 1, b) AP3

a)   b)   c)
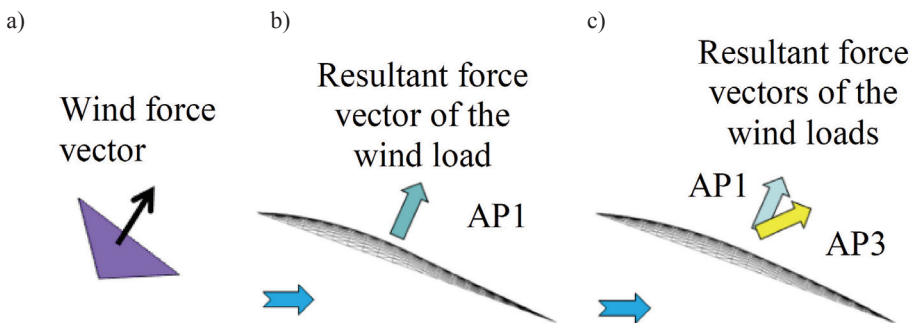

Fig. 18. Comparison of the total load vectors between AP1 and AP3, wind direction $\theta = 0°$, F2 model of the mono-slope roof, a) triangle element in FEM, b) AP1, c) AP3

Comparison of the total reaction forces between AP1 and AP3 of the mono-sloped roof

		Wind direction $\theta = 0°$	
		AP1	AP3
F1	Reaction force X (kN)	−61	−61
	Reaction force Z (kN)	−169	−169
	Moment Y (kNm)	−322	−332
F2	Reaction force X (kN)	−52	−56
	Reaction force Z (kN)	−171	−170
	Moment Y (kNm)	−133	−142

5. Effect of roof deformation on wind forces

5.1. Analytical method

Because the membrane canopy roof structures are generally flexible, they may deform significantly under wind loading. The deformation may affect the flow pattern around the roof structure and change the wind loads on it, which in turn will cause additional deformation of the roof structure. The present paper focuses on the effect of static deformation on the time-averaged wind forces. In fact, the dynamic fluid-structure interaction (FSI), represented as aerodynamic damping and stiffness, may affect the response of the roof significantly in some cases. This will be the subject of a future study.

The effect of the roof deformation of flexible roofs on the wind force coefficients was investigated by computational fluid dynamics (CFD) and structural analysis [7, 8]. We focussed only on the time-averaged values of the wind forces and structural responses. The procedure that we followed consisted of the following steps. Firstly, the wind force coefficients acting on the rigid roof were obtained by CFD analysis using the Reynolds averaged Navier–Stokes model (Step 1). Secondly, using the wind force coefficients obtained at Step 1, we computed the roof deformation (Step 2). Thirdly, we computed the wind force coefficients acting on the deformed roof (Step 3). Finally, we used the wind force coefficients obtained at Step 3 to compute the roof deformation (Step 4). This procedure was repeated until the load effects converged to constant values (Fig. 19). Here, we used $G_f = 1.0$ because the focus was only on the time-averaged values. In practice, membrane roofs vibrate under dynamic wind loads; however, the effects are not considered in the present analysis. Referring to the Japanese design standard for steel structures, the criterion for convergence is based on the variation of the deformed roof shape,

$$\frac{\delta_n - \delta_{n-1}}{a} \le \frac{1}{300} \tag{19}$$

where δ_n and δ_{n-1} represent the maximum displacement at the n and $n−1$ step, respectively.

We used the open-source code named OpenFOAM, version 1.5, released in 2008. The wind tunnel experiments were simulated. The computational domain for the mono-sloped roof was 1.0 m wide, 1.0 m high and 3.0 m long and for the HP roofs, it was 1.0 m wide, 1.4 m high and 3.0 m long. The roof models were placed at the same configuration as that used in the wind tunnel experiments. Fig. 20 shows the numerical model of the mono-sloped roof with the initial shape. The computation is based on the finite-volume method, in which the semi-implicit method for pressure-linked equations (SIMPLE) algorithm and the renormalization group k-ε (RNG k-ε) model are used. The boundary conditions are summarized in Tab. 9. The turbulence intensity I_u for the analysis was determined based on the wind tunnel experiment (Fig. 21).
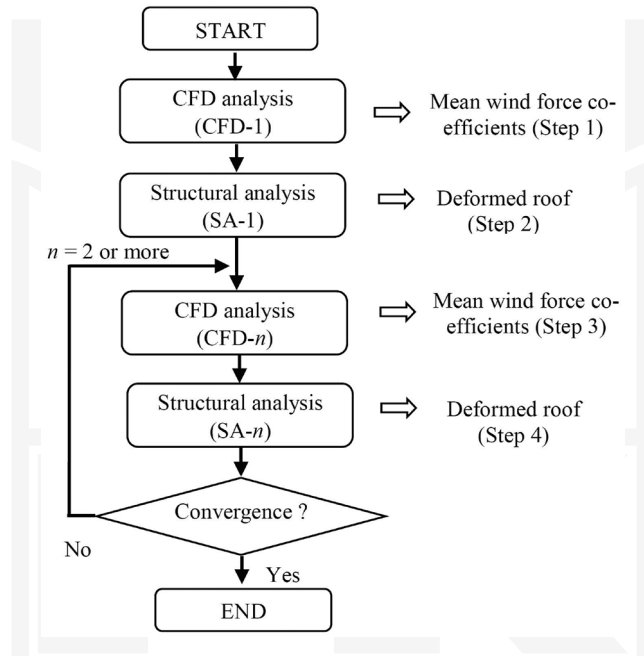

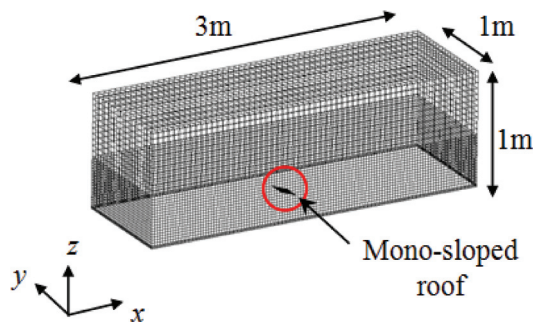Fig. 19. Procedure for investigating the effect of roof deformation due to mean wind load

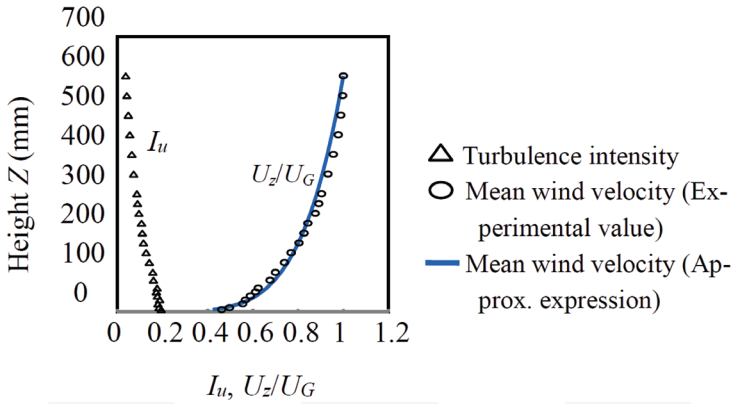Fig. 20. Numerical model for the mono-sloped roof

Fig. 21. Profiles of turbulence intensity I_u and mean wind velocity normalized by the value at a height of $Z_G = 600$ mm, U_G – mean wind velocity at the reference height of $Z_G = 600$ mm

Table 9

Boundary conditions in the simulated wind tunnel

Surface at X_{min} (Inlet)	<Power law > $$U_Z = U_G \left\{ \frac{Z}{Z_G} \right\}^\alpha$$ Reference height: $Z_G = 0.6$ m Wind velocity at the reference height: $U_G = 8$ m/s Power law index: $\alpha = 0.18$ Turbulence intensity: experimental values (Fig. 21)
Surface at X_{max} (Outlet)	Surface pressure at outlet: 0 Pa
Surface at Y_{min}, Y_{max} and Z_{max}	Free-slip wall
Surface at Z_{min}	No-slip wall
HP surface	No-slip wall

5.2. Roof deformation and mean wind forces

Figs. 22a–22c and 23a–23c show the roof deformations at Step 4 for the mono-sloped and HP-shaped roofs, respectively. Figs. 24a–24d and 25a–25d show the ratio of stress at Step 4 to that at Step 2 for the mono-sloped and HP- shaped roofs, respectively. As might be expected, the ratio is generally small for the F1 model because the roof deformation is relatively small. In contrast, the ratios for the F2 and S1 models are generally larger than that for the F1 model; the largest value is approximately 1.2 for the F2 model (Fig. 24a). This feature may be related to the stiffness and arrangement of the members. Moreover, the difference in the

185

structural system between frame and suspension types may cause a difference in the stress ration between models. These results suggest that previously proposed design wind force coefficients cannot be applied to flexible roofs.
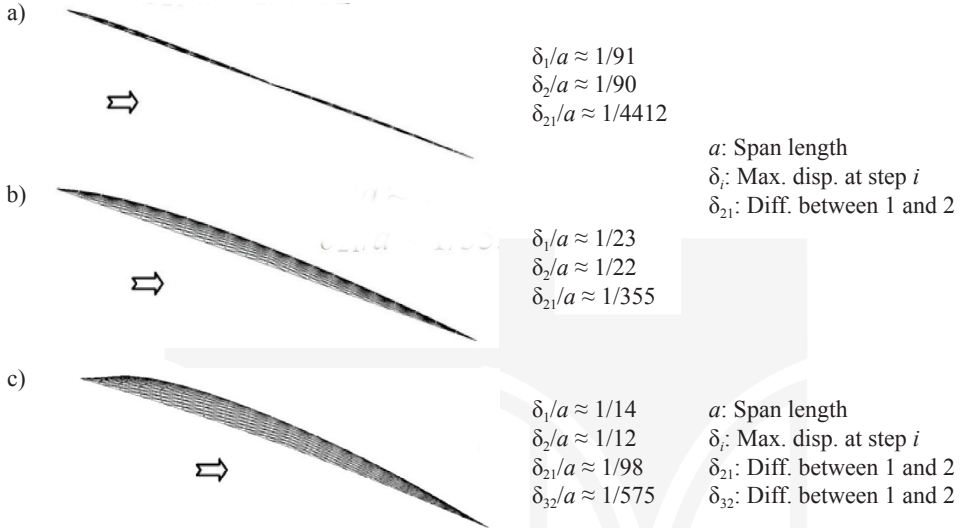
a)

$\delta_1/a \approx 1/91$
$\delta_2/a \approx 1/90$
$\delta_{21}/a \approx 1/4412$

a: Span length
δ_i: Max. disp. at step i
δ_{21}: Diff. between 1 and 2

b)

$\delta_1/a \approx 1/23$
$\delta_2/a \approx 1/22$
$\delta_{21}/a \approx 1/355$

c)

$\delta_1/a \approx 1/14$ a: Span length
$\delta_2/a \approx 1/12$ δ_i: Max. disp. at step i
$\delta_{21}/a \approx 1/98$ δ_{21}: Diff. between 1 and 2
$\delta_{32}/a \approx 1/575$ δ_{32}: Diff. between 1 and 2

Fig. 22. Deformation of the mono-sloped models (wind direction θ = 0°). Scale factor for displacement: one time. a) F1 model, b) F2 model, c) S1 model

a)

$\delta_1/a \approx 1/143$
$\delta_2/a \approx 1/135$
$\delta_{21}/a \approx 1/2500$

b)

$\delta_1/a \approx 1/76$
$\delta_2/a \approx 1/67$
$\delta_{21}/a \approx 1/600$

c)

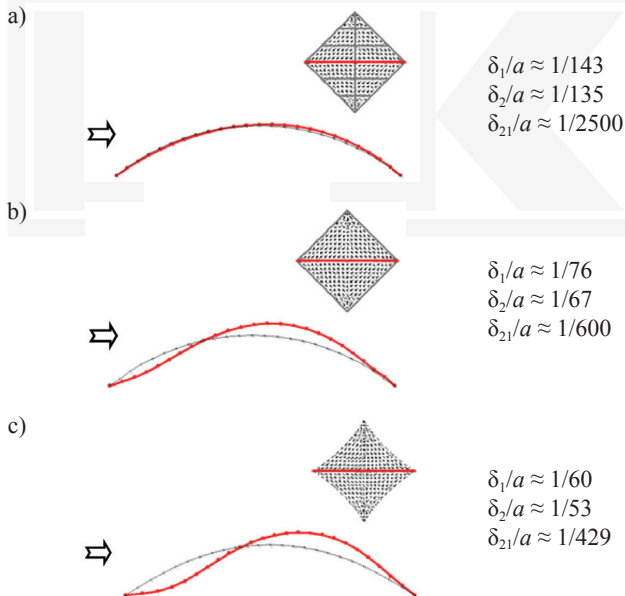$\delta_1/a \approx 1/60$
$\delta_2/a \approx 1/53$
$\delta_{21}/a \approx 1/429$

Fig. 23. Deformation of the HP-shaped models (wind direction θ = 0°). Scale factor for displacement: five times. a) F1 model, b) F2 model, c) S1 model
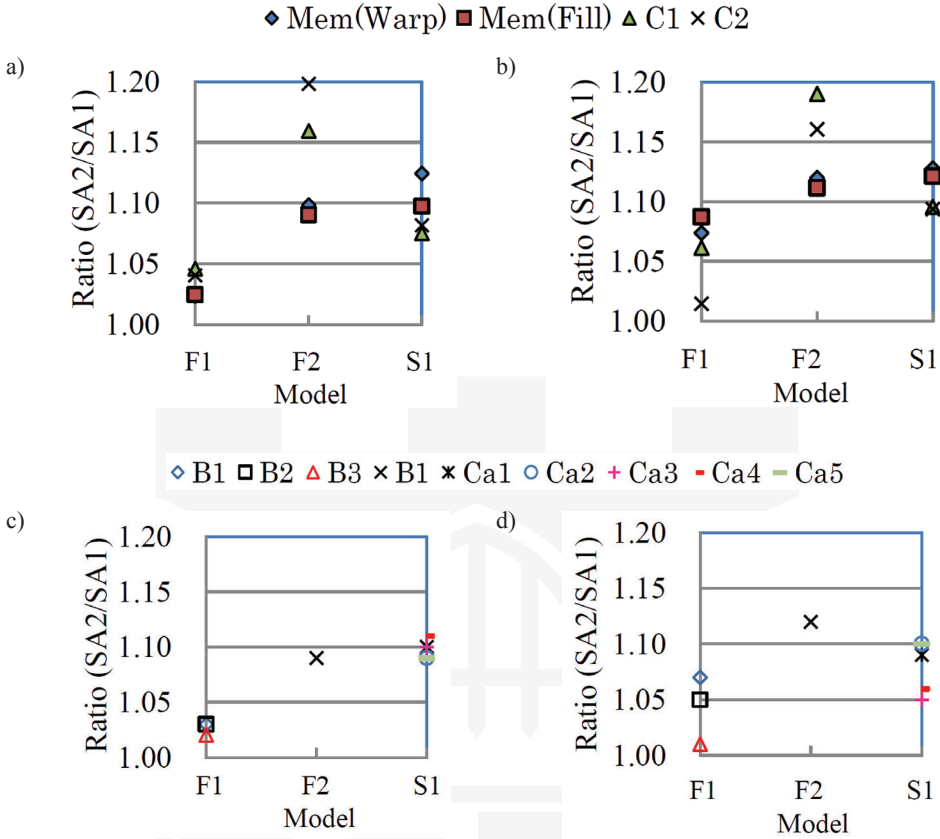
Fig. 24. Ratio of the maximum stress obtained from SA-2 to that obtained from SA-1 for the mono-sloped models, a) wind direction θ = 0°, b) wind direction θ = 180°, c) wind direction θ = 0°, d) wind direction θ = 180°

6. Design wind force coefficients for membrane-free roofs

The results in Chapters 4 and 5 suggest that the design wind force coefficients proposed based on the results of wind tunnel experiments with rigid models should be improved by considering the effect of the roof-supporting systems and roof deformation on the membrane structure load. The simplest formula of the wind force coefficients may be given by the following equations:

$$C_{NW}^* = \frac{\gamma \mu C_{NW0}}{G_f} \qquad C_{NL}^* = \frac{\gamma \mu C_{NL0}}{G_f} \qquad (20)\,(21)$$
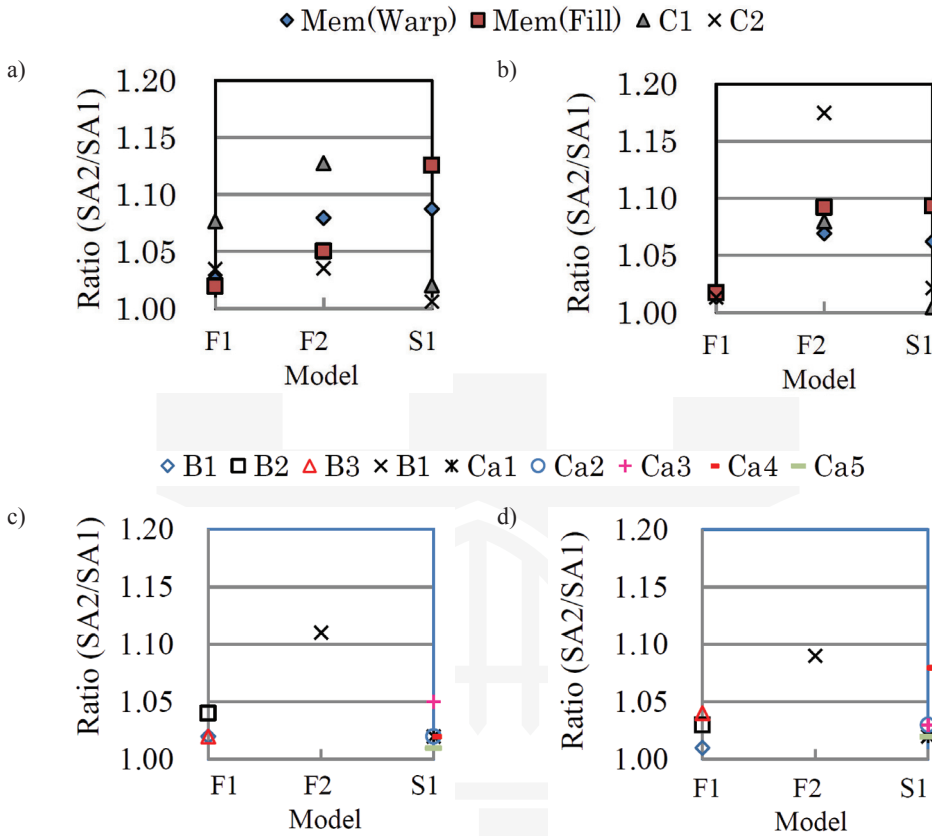
Fig. 25. Ratio of the maximum stress obtained from SA-2 to that obtained from SA-1 for the HP-shaped models, a) wind direction $\theta = 0°$, b) wind direction $\theta = 90°$, c) wind direction $\theta = 0°$, d) wind direction $\theta = 90°$

where μ represents a correction factor for membrane roofs and may be given by

$$\mu = \mu_s \times \mu_d \tag{22}$$

where μ_s and μ_d represent correction factors for the roof-supporting system and roof deformation, respectively.

An appropriate value of μ_s may be determined from the results of the structural analysis investigating the effect of the roof-supporting systems on the load effects (Chapter 4). The stress ratios for the mono-sloped and HP-shaped roofs are summarized in Tables 6 and 7, respectively. In most cases, the ratio is nearly equal to or less than 1.1. Therefore, an appropriate value of μ_s may be 1.1. Actually, the maximum value of the stress ratio is 1.32 for the B3 member of the F1 model (see Table 7). The B3 member is located along the boundary of the leeward and windward halves (Fig. 26). The design wind force coefficient changes discontinuously along the boundary line, whereas the actual wind force coefficient changes

smoothly. The discontinuous change in the wind force coefficient along the B3 member may induce a large unbalanced force on the member, resulting in a large stress ratio that may be unrealistic.

Regarding the μ_d value, based on the results of the CFD and structural analysis on the effect of roof deformation (Chapter 5), an appropriate value of μ_d may be approximately 1.2, which was obtained from the results in Figs. 24 and 25. Using the above-mentioned μ_s and μ_d values, the correction factor μ for membrane roofs is ~1.3 within the limits of the present study.
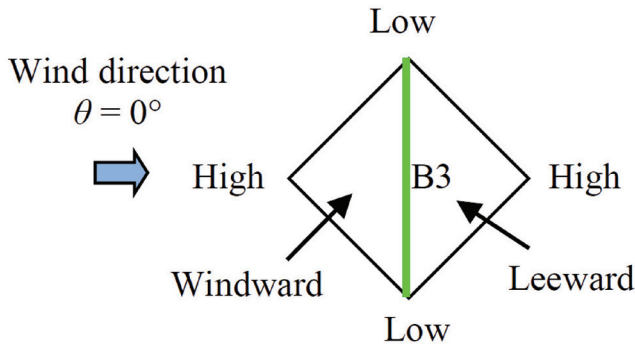

Fig. 26. B3 member of the F1 model for the HP-shaped roof

7. Concluding remarks

The present study has presented wind force coefficients for designing free-standing canopy roofs of membrane structures. The membrane roofs are so lightweight and flexible that the roof easily deforms under wind loading. In addition, there are various roof-supporting systems for membrane structures. In a previous study, we proposed the design wind force coefficients based on the results of wind tunnel experiments with rigid roof models. The proposed wind force coefficients was obtained assuming that four corner columns supported the roof and the roof deformation could be neglected. The axial forces induced in the columns were considered as the most important load effect. In this study, however, we show that the previously proposed design wind force coefficients are inappropriate for designing flexible membrane roofs and should be improved. It is also shown that load effects such as the bending moment should be considered when discussing the design wind force coefficients. Among the many roof configurations, we focused on mono-sloped and hyperbolic paraboloid (HP)-shaped roofs. The effects of roof deformation and roof-supporting systems of those roofs on the wind force coefficients were investigated. Based on the results of the investigation, we have introduced a correction factor (μ) in the previously proposed wind force coefficients. The μ is given by $\mu = \mu_s \times \mu_d$. The μ_s and μ_d represent correction factors for the roof-supporting system and roof deformation, respectively. The correction factor μ is ~1.3 within the limits of the present study.

R e f e r e n c e s

[1] Michalski A., Britto D., Gelenne Ph., Haug E., *Fluid structure interaction simulation of wide-span membrane structures,* Extended Abstracts of the 6th International Symposium on Computational Wind Engineering Hamburg, Germany 8-12 June 2014.

[2] Michalski A., Kermel P.D., Haug E., Lohner R., Wuchner R., Bletzinger K.-U., *Validation of the computational fluid-structure interaction simulation at real-scale tests of a flexible 29 m umbrella in natural wind flow,* Journal of Wind Engineering and Industrial Aerodynamics, Vol. 99, 2011, 400-413.

[3] Nagai Y., Okada A., Kanda M., Miyasato N. and Saitoh M., *Study on wind response on horn-shaped membrane structure,* Journal of Structural and Construction Engineering, AIJ, Vol. 77(672), 2012, 211-219.

[4] OpenFOAM, http://www.openfoam.com, 2008.

[5] Pun P.K.F., Letchford C.W., *Analysis of a tension membrane hypar roof subjected to fluctuating wind loads,* Proc 3rd Asia-Pacific Symposium on Wind Engineering, Hong Kong, 13-15 December 1993.

[6] Takeda F., Yoshino T., Uematsu Y., *Design wind force coefficients for hyperbolic paraboloid free roofs,* Journal of Physical Science and Application 4(1), 2014, 1-19.

[7] Takeda F., Yoshino T., Uematsu Y., *Discussion of design wind force coefficients for hyperbolic paraboloid free roofs*, Proc. 7th International Colloquium on Bluff Body Aerodynamics and Applications, Shanghai, China 2012.

[8] Takeda F., Yoshino T., Uematsu Y., *Discussion of design wind force coefficients on mono-sloped free roofs*, Proc. of the International Association for Shell and Spatial Structures (IASS) Symposium, Seoul, Korea, 2012.

[9] Uematsu Y., Arakatsu F., Matsumoto S., Takeda F., *Wind force coefficients for the design of a hyperbolic on wind engineering*, Taipei, Taiwan 2009.

[10] Uematsu Y., Iizumi E., Stathopoulos T., *Wind loads on free-standing canopy roofs: Part 2 overall wind forces,* Journal of Wind Engineering and Industrial Aerodynamics, Vol. 96 (6-7), 2008, 1029-1042.